Lignin Functionalized with Succinic Anhydride as Building Block for Biobased Thermosetting Polyester Coatings

Carmela Scarica, Raffaella Suriano[ID], Marinella Levi, Stefano Turri[ID], and Gianmarco Griffini*[ID]

Department of Chemistry, Materials and Chemical Engineering “Giulio Natta”, Politecnico di Milano, Piazza Leonardo da Vinci 32, 20133 Milano, Italy

ABSTRACT: Novel lignin-based thermosetting polyester (PE) coating systems are presented in this work. These new materials are based on the functionalization of a soluble fraction of softwood kraft lignin recovered from solvent extraction with increasing amounts of succinic anhydride (SAn), to obtain SAn/lignin adducts via the formation of ester bonds on the hydroxyl groups in lignin. A thorough chemical, physical, and thermal characterization of the resulting esterified materials was conducted to confirm the successful covalent incorporation of SAn in the lignin macromolecule. Such function-alized SAn/lignin adducts were employed as building blocks for the preparation of cross-linked lignin-based PE coatings under different curing conditions. These PE coatings highlighted improved thermal stability, film forming ability, solvent resistance, dynamic surface hardness, and higher hydrophobic character compared with the unmodified parent lignin precursor. In addition, the adhesion strength of these systems on different substrates was also assessed. The results of this study demonstrate an easily accessible approach to develop high-lignin-content thermosetting PE systems and provide evidence of the potential of these materials as bioderived coatings and adhesives.

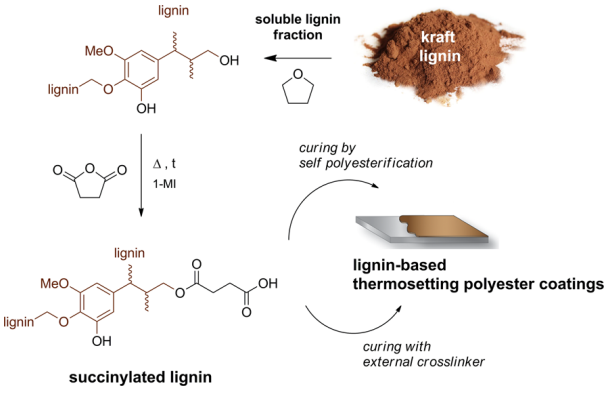

Keywords: Lignin, Polyesters, Biobased, Coating, Adhesive

INTRODUCTION

Lignocellulose is the major structural component of plant-based biomass and represents one of the most abundant renewable resources on the planet, with over 75 billion tonnes available annually. Lignocellulosic biomass is mainly constituted by three biopolymeric compounds, namely cellulose (35−83% dry weight basis), hemicellulose (0−30% dry weight basis), and lignin (1−43% dry weight basis), in addition to minor amounts of other species (xylose, arabinose, tannin).[1−3] In particular, lignin represents the most abundant naturally occurring source of aromatics on Earth, accounting for about 30% of all nonfossil organic carbon. Currently, one of the main sources of lignin production is the pulp and paper industry, where it is typically recovered as waste material during pulping treatments. The end-of-life scenario for such isolated lignin is typically its use as low-cost fuel for power production and heat recovery, while only a minor fraction is utilized in niche market applications that include formulations for dispersants, adhesives, surfactants, or antioxidants for plastics and rubbers.[4−6] The limited exploitation of such a widespread renewable resource urgently calls for efficient approaches to enhance lignin utilization as precursor for the design and production of materials with increased commercial and technological value.

In this context, the high concentration of functional groups (mainly hydroxyls) in lignin can be exploited for the development of different classes of lignin-based copolymers, including phenolics, epoxies, polyurethanes, and polyesters.[7−15] Among these, polyesters (PEs) represent a particularly interesting class of materials that have been successfully employed in several industrial fields for a wide variety of applications thanks to their high versatility and easily tunable chemical and physical properties, including potential biodegradability.[16] Therefore, the use of lignin as building block for the development of high-performance biobased PEs is of great scientific and technological interest, particularly considering the aromatic nature of such naturally occurring material combined with its relatively large abundance of reactive functionalities.

Some of the early works on lignin-based PEs were based on the functionalization of lignin with dicarboxylic acid chlorides in the presence of additional polyols.[17−19] These approaches were found to primarily yield cross-linked systems as a result of the high functionality of lignin, although examples of thermoplastic materials were also reported, in some cases amenable to hot-melt processing.[20−23] More recently, esterification of lignin has been successfully demonstrated by reaction with different carboxylic diacids and anhydrides of varying chain length. These modifications have yielded materials with tunable (typically lower than lignin) glass

Received: October 5, 2017
Revised: January 9, 2018
Published: January 12, 2018

Corresponding Author

*E-mail: gianmarco.griffini@polimi.it. Tel: +39 022399 3213. **ORCID**
Raffaella Suriano: 0000-0002-7448-359X
Stefano Turri: 0000-0001-8996-0603
Gianmarco Griffini: 0000-0002-9924-1722

Scheme 1. Schematic Representation of the Functionalization Reaction between the THF-Soluble Lignin Fraction and SAn To Lead to Succinylated Lignin

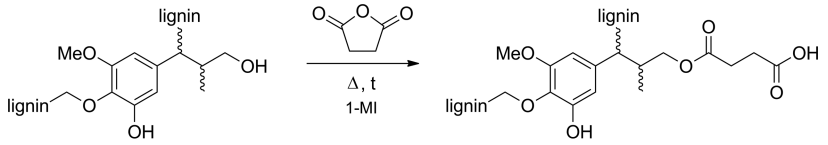

soluble lignin fraction succinylated lignin

transition temperature (T_g), improved solubility in organic solvents and enhanced reactivity through the incorporation of more accessible pendant carboxylic moieties covalently attached to the lignin macromolecule.[24] This approach has been widely employed to improve the compatibility of lignin as filler in polymer-based (mainly polyolefinic) composite systems.[25−28] Conversely, very little has been done on the use of esterified lignin adducts as reactive cross-linkable precursors for the development of lignin-based PE materials.[29] In this context, the reaction of lignin with succinic anhydride (SAn) has remained relatively unexplored compared to other anhydride-based systems, even though SAn has already been extensively utilized in its alkenyl derivative form in the pulp and paper industry as paper sizing agent.[30,31] In addition, SAn may also be amenable to green biotechnological routes for its preparation.[32,33] In this context, only a few studies have reported on the succinylation of lignin with SAn,[34,35] with main application in cross-linking reactions with epoxy systems.[36−39] However, to date no examples have appeared in the literature on the use of SAn-functionalized softwood lignin for the preparation of cross-linked PE coatings.

To bridge this gap, novel lignin-based thermosetting PE coating systems are presented in this work, based on the functionalization of softwood lignin with SAn. Different SAn/lignin (SAL) adducts were obtained and subsequently employed as macromolecular building blocks for the preparation of fully cross-linked lignin-based PE coatings.

The results of this study suggest a straightforward strategy to develop new high-lignin-content PE thermosetting systems that may find application as bioderived coatings and adhesives.

EXPERIMENTAL SECTION

Materials. The softwood kraft lignin used in this work (Indulin AT, from here on referred to as KL) was provided by MeadWestvaco. Succinic anhydride (SAn), 1-methylimidazole (1-MI), tetrahydrofuran (THF), methyl ethyl ketone (MEK), *p*-toluene sulfonic acid (PTSA) and sodium hypophosphite (NaHP) were supplied by Sigma-Aldrich and used as received. The hexamethoxy methylmelamine-based cross-linking agent (Cymel 303, from here on referred to as HMMM) was supplied by Cytec Industries.

Synthesis of SAn-based lignin adducts. Since most lignins are only partially soluble in common organic solvents and most modifications require organic solvents as reaction media, lignin dissolution is a key step for allowing further reactions. For this reason, KL was preliminarily fractionated by means of THF following a procedure described in our previous work[40] and a dry THF-soluble fraction (from here on referred to as SLF) was recovered for further processing (60% fractionation yield).

For the esterification reaction, SLF and SAn were dissolved in THF in the presence of 1-MI catalyst (0.05 mL/g SLF) in a three-neck round-bottom flask and allowed to vigorously stir for 3 h at 60 °C under gentle reflux. In order to investigate the effect of the amount of SAn on the chemical-physical characteristics of the resulting SAL adducts, four different SAn/lignin weight ratios were investigated, namely 10 wt % (SAL10, 1 mmol SAn/1 g lignin), 15 wt % (SAL15, 1.5 mmol SAn/1 g lignin), 20 wt % (SAL20, 2 mmol SAn/1 g lignin) and 25 wt % (SAL25, 2.5 mmol SAn/1 g lignin). In addition, to assess the potential effect of reaction time on the reaction conversion, the esterification reaction on SAL25 was conducted for both 3 and 7 h. Upon completion, the solvent was removed by rotary evaporation and the samples dried under vacuum for 24 h. A schematic representation of the functionalization process is shown in Scheme 1. To ensure reproducibility, each esterification reaction was performed at least in triplicates and each characterization carried out on the SAL adducts as well as on the resulting cross-linked materials was repeated at least twice, unless otherwise stated.

Preparation of cross-linked coatings. In order to prepare SAL-based cross-linked coatings, two different strategies were adopted. The first approach consisted in the cross-linking reaction of SAL20 with HMMM external curing agent using PTSA as catalyst (0.5 wt % on total solid content) at three different SAL/HMMM weight ratios, namely 93/7 (SAL-H7), 95/5 (SAL-H5) and 97/3 (SAL-H3). In the second approach, SAL20 was allowed to undergo a self-polyesterification reaction in the presence of NaHP as catalyst (the so-obtained material will be referred to as SAL-S). In both cases, coatings were prepared by depositing the precursor solutions (20 wt % dry content in MEK) onto the target substrate (glass, wood and aluminum) by means of a WS-400B-NPP Spin-Processor (Laurell Technologies Corp.). After spin coating deposition (600 rpm, 40 s), all samples were thermally treated at 200 °C for 30 min in a ventilated oven to allow the cross-linking reaction to occur. The effectiveness of the cross-linking process was verified by MEK test (pass 100 double rubs, ASTM D4752).

Characterization. *Gel permeation chromatography (GPC).* The molecular weight of all esterified lignin samples was estimated by means of gel permeation chromatography (GPC) using a Waters 510 HPLC system equipped with a Waters 486 Tunable Absorbance Detector set at λ = 300 nm, using THF as eluent. The sample (200 μL of esterified lignin in THF, 1 mg/mL) was injected into a system of columns connected in series (Ultrastyragel HR, Waters) and the analysis was performed at 30 °C and at a flow rate of 0.5 mL/min. The GPC system was calibrated against polystyrene standards in the 10^2−10^4 g/mol molecular weight range.

Fourier-transform infrared spectroscopy (FTIR). The monitoring of the esterification reactions as well as the chemical characterization of the synthesized materials were performed by means of Fourier-transform infrared (FTIR) spectroscopy by means of a Nicolet 760 FTIR Spectrophotometer on samples dissolved in THF and deposited on NaCl disks by spin coating. FTIR spectra were recorded in transmission mode at room temperature in air by recording 32 accumulated scans at a resolution of 2 cm^{-1} in the 4000−700 cm^{-1} wavenumber range.

Quantitative ^{31}P NMR spectroscopy. ^{31}P NMR spectra were recorded by inverse gated proton decoupling sequences on a Bruker Avance 500 spectrometer with 5 mm direct detection broadband probe-head. The spectra were collected at 27 °C with 384 transients using 90° pulse flip angle, 1 s acquisition time, and 5 s relaxation delay. Prior to analysis, samples (KL, SLF and SAL20) were dried overnight in a vacuum oven at 40 °C and then derivatized according to a procedure described in the literature.[41] The phosphitylation reagent was 2-chloro-4,4,5,5-tetramethyl-1,3,2-dioxaphospholane, the internal standard was *N*-hydroxy-5-norbornene-2,3-dicarboxylic acid imide and the relaxation agent was chromium(III) acetylacetonate (all purchased from Sigma-Aldrich). The integration regions were: internal standard

152.8−152.5, aliphatic hydroxyls 150.0−145.0, phenolic hydroxyls 145.0−137.0, and carboxylic hydroxyls 137.0−134.5.

Differential scanning calorimetry (DSC). Differential scanning calorimetry (DSC) was employed to investigate the thermal transitions in the prepared samples. Measurements were conducted on 6−9 mg samples by means of a Mettler-Toledo DSC/823e instrument by performing three runs (heating/cooling/heating) from 25 to 200 °C at a scan rate of 20 °C/min under nitrogen flux. The T_g of the materials was evaluated as inflection point in the second heating run. In the case of SAL-based cross-linked materials, the coatings were prepared on glass slides and then scraped off as powder prior to analysis.

Thermogravimetric analysis (TGA). Thermogravimetric analysis (TGA) was performed on solid state samples (10−15 mg) by means of a Q500 TGA system (TA Instruments) from ambient temperature to 600−800 °C at a scan rate of 10 °C/min both in air and under nitrogen flux. In the case of SAL-based cross-linked materials, the coatings were prepared on glass slides and then scraped off as powder prior to analysis.

Optical contact angle. Static optical contact angle measurements on the PE coatings were performed with an OCA 20 (DataPhysics) equipped with a CCD photocamera and a 500-μL Hamilton syringe to dispense liquid droplets. Measurements were taken at room temperature via the sessile drop technique. At least 20 measurements were performed in different regions on the surface of each sample and results were averaged. Water and diiodomethane were used as probe liquids.

Dynamic hardness measurements. Dynamic hardness measurements were carried out with a NSCRIPTOR system using a Bruker DNISP nanoindentation probe, consisting of a diamond tip mounted on a stainless steel cantilever (calibrated spring constant certified by supplier k = 195 N/m). Measurements were performed by applying an average normal load of 66 μN, which was controlled by calibrating the deflection sensitivity of the DNISP probe, as previously explained.[42] Such value of applied load was also selected in order to avoid producing deep scratches with a penetration depth higher than 10% of the thickness of the pristine coatings. Nanoscratches were obtained using a lithographic software (Nanoink's InkCAD) and setting a scratch length of 14 μm and a scratching rate of 0.1 μm/s and 10 μm/s. The dynamic hardness of the coatings was obtained based on the applied load and on the width of the resulting scratch groove (please refer to Supporting Information for a detailed description of the procedure adopted).[43,44]

Adhesion tests. The adhesive properties of the cross-linked SAL-based PE materials on different substrates (glass, wood, aluminum) were evaluated by employing a PosiTest AT-M Manual adhesion pull-off tester (DeFelsko) by measuring the pulling force needed to detach a 20 mm-diameter aluminum dolly glued to the PE films by means of a two-component epoxy adhesive (Araldite 2011, curing cycle: 50 °C, 24 h).[45]

RESULTS AND DISCUSSION

Gel permeation chromatography (GPC) on SAn-based lignin adducts. To evaluate the effect of the esterification reaction on the molecular weight distribution of the resulting lignin-based materials, the molecular weight of all succinylated adduct systems (SAL10 to SAL25) as well as of the unmodified THF-soluble lignin fraction (SLF) was determined by GPC analysis. All materials show a broad molecular weight distribution with a partially bimodal profile (see Supporting Information), in agreement with previous works.[13] In addition, by increasing the SAn/SLF ratio, a progressive shift of the GPC chromatograms of SAL systems toward longer retention times is reproducibly observed compared to the SLF, accompanied by a slight broadening of their molecular weight distribution. As presented in Table 1, the SLF sample shows M_n, M_w, and polydispersity index (PDI) values of 1090 g/mol, 1800 g/mol, and 1.7, respectively, while higher molecular weights and PDIs are observed on all SAL systems. In particular, both M_n and M_w are found to increase with the concentration of SAn in the lignin adduct up to a maximum observed for SAL20 (M_n = 1270 g/mol, M_w = 2800 g/mol, PDI = 2.2), while higher SAn concentrations do not lead to further significant modifications. This behavior may be explained by considering that lignin possesses a limited amount of hydroxyl groups readily available for functionalization.[13] Upon succinylation reaction of such −OH moieties, an increase in molecular weight is consistently observed, as lateral chains (from SAn) are added to the main lignin macromolecular backbone. This evidence give a preliminary indication of successful incorporation of SAn into lignin. However, once all available −OH groups have reacted with SAn, no further functionalization reaction can occur on lignin due to the lack of accessible hydroxyl groups. As a result, the molecular weight of SAL-based adducts with high SAn concentration (>20 wt %) is found not to increase further.

Table 1. Molecular Weights (M_n and M_w) and Polydispersity Index (PDI) of the THF-Soluble Lignin Fraction (SLF) and of All SAn-Based Adducts Obtained in This Work (SAL10, SAL15, SAL20, SAL25)

	SAn concentration in the reaction feed (wt %)	M_n [g/mol]	M_w [g/mol]	PDI
SLF		1090	1800	1.7
SAL10	10	1120	2000	1.8
SAL15	15	1180	2150	1.8
SAL20	20	1270	2800	2.2
SAL25	25	1250	2310	1.9

Fourier-transform infrared spectroscopy (FTIR) on SAn-based lignin adducts. The chemical modifications occurring to lignin upon esterification were evaluated by means of FTIR spectroscopy. As shown in Figure 1, where the FTIR spectra of all investigated lignin-based systems are reported, the pristine SLF material exhibits the characteristic signals of softwood kraft lignin.[41,46] Upon esterification, a decrease in the intensity of the −O−H stretching band at 3400 cm^{-1} compared to pristine SLF is observed for all samples, indicating a reduction of the native hydroxyl group concentration in lignin following the reaction with SAn. In addition, a broadening of the signal in the 3400−3000 cm^{-1} spectral region is observed, which may be ascribed to the −OH stretching vibrations in the terminal −COOH groups forming after reaction between lignin and SAn. Similarly, a major band is found to appear at 1730 cm^{-1} whose intensity increases with increasing the SAn/SLF ratio. This C═O stretching vibration signal, not present in the pristine SLF material, results from the formation of new carbonyl groups linked to lignin as ester moieties and clearly suggests successful covalent incorporation of SAn into lignin via ester bonds. Further evidence for the successful formation of the SAn−lignin adducts is the increase in intensity of the absorption bands in the 1250−1100 cm^{-1} region compared to SLF, where signals associated with C−C, C−O, and C═O stretching vibrations in esters can be typically found. It is interesting to note that, for high SAn/lignin ratios (SAL25), some characteristic FTIR signals attributable to bond vibrations in succinic anhydride can be observed, likely suggesting the presence of unreacted SAn in the reaction product. In particular, a weak peak centered at 1860 cm^{-1} and a shoulder at 1780 cm^{-1} can be detected in the FTIR spectrum of SAL25, ascribable to symmetric and asymmetric stretching vibrations of C═O in SAn, respectively (Supporting Information). Concurrently, two additional peaks are also

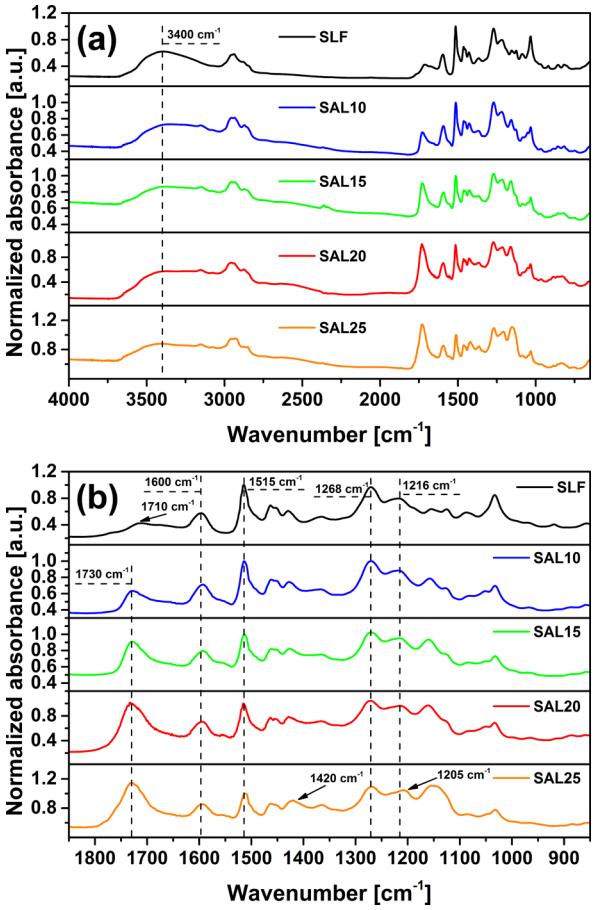

Figure 1. (a) FTIR spectra of the THF-soluble lignin fraction (SLF) and of all SAn-based adducts obtained in this work (SAL10, SAL15, SAL20, SAL25); (b) zoomed FTIR spectra in the 1800−900 cm^{-1} region.

observed attributable to vibrations of C−O (1420 cm^{-1}) and C−O−C and CH_2 (1205 cm^{-1}) bonds in SAn. On the contrary, no residual FTIR signals associated with SAn are detected in SAL10, SAL15, and SAL20. Based on these results, an attempt was made to further boost the reaction conversion in the case of SAL25 by increasing the succinylation reaction time up to 7 h. However, no beneficial effects on the reaction product were observed, as residual FTIR signals assigned to unreacted SAn could still be detected even after 7 h of esterification reaction (data not shown). Accordingly, no further characterizations were performed on SAL25. This evidence may suggest that under the conditions employed in this work only a limited portion of all −OH groups present in SLF is available for reaction with SAn, as will be discussed in the next section.

Quantitative ^{31}P NMR analysis. The evaluation of the number of reactive hydroxyl groups in lignin was performed by means of quantitative ^{31}P NMR spectroscopy. Based on the preliminary FTIR analysis previously discussed, SAL20 was found to be the functionalized system in which the highest content of anhydride could be incorporated without leading to the presence of unreacted SAn in the reaction product. For this reason, it was selected as the target system to quantify the maximum amount of hydroxyl groups in lignin available for reaction with SAn (^{31}P NMR spectra are reported in the Supporting Information). As shown in Table 2, after lignin fractionation with THF, the total hydroxyl content in the

Table 2. Amount of Hydroxyl (aliphatic and phenolic) and Carboxylic Groups in Parent Lignin (KL), THF-Soluble Fraction (SLF), and SAn-Based Adduct SAL20[a]

	OH (aliphatic)	OH (phenolic)	OH total	COOH
KL	1.65	3.25	4.90	0.17
SLF	1.65	4.10	5.75	0.23
SAL20	0.12	3.38	3.50	1.46

[a]As obtained from quantitative ^{31}P-NMR spectroscopy (values are expressed in terms of mmol/g with an error of ±0.1 mmol/g).

resulting soluble fraction SLF was 5.75 mmol/g (1.65 mmol aliphatic OH/g, 4.10 mmol aromatic OH/g). Upon functionalization with SAn (2 mmol SAn/g SLF), such hydroxyl groups were found to decrease down to 3.50 mmol/g, as a result of the esterification reaction. In particular, most aliphatic OH groups in SLF were found to be consumed during the functionalization with SAn, leading to a residual amount of 0.12 mmol aliphatic OH/g. On the other hand, only a minor decrease was observed in phenolic OH groups. These results are in line with recent literature reports[47] in which it was also demonstrated that aliphatic hydroxyls exhibit higher reactivity compared to phenolic ones during the esterification reaction. Overall, a total consumption of 2.25 mmol OH/g was observed during succinylation, which is in line with the molar amount of SAn loaded in the reaction feed (2 mmol SAn/g SLF).[26] Besides the consumption of hydroxyls, an increase of number of COOH groups is also observed upon functionalization (1.46 mmol COOH/g in SAL20), which is consistent with the appearance of new carboxylic moieties as a result of the incorporation of SAn in the lignin macromolecule.

Thermal characterization of SAn-based lignin adducts. The thermal transitions of the SAn-based lignin adducts were investigated by means of DSC analysis. As shown in Figure 2a, all SAL systems exhibit a lower glass transition temperature (T_g) compared to the unmodified SLF lignin. In particular, a progressive decrease in T_g is observed by increasing the SAn/SLF ratio, leading to values of 84 °C, 77 °C, and 69 °C for SAL10, SAL15, and SAL20, respectively. In agreement with previous studies on esterified lignin,[26,34] this evidence indicates that SAn may act as internal plasticizer for lignin, due to the increased molecular mobility resulting from the addition of progressively higher amounts of the linear ester chain to the bulky lignin core as lateral substituent.

TGA measurements were carried out to analyze the effect of succinylation on the thermal stability of the resulting lignin-based adducts (Figure 2b). The parent SLF material exhibits a three-stage thermal degradation profile with major mass loss events peaked in the 25−150 °C, 150−300 °C, and 300−500 °C temperature ranges. The first mass loss can be associated with evaporation of trapped solvent and water, and it leads to a mass reduction of about 10−15%. The second thermolytic degradation step yields a further 10−15% mass loss and can be ascribed to the breaking of α- and β-aryl-alkyl-ether linkages, aliphatic chains, and decarboxylation reactions.[48] The third high-temperature (>300 °C) mass loss event may result from the rupture of intramolecular carbon−carbon linkages.[49] After reaction with SAn, a general improvement of the thermolytic resistance is observed on all functionalized systems at temperatures lower than 250 °C. In particular, the temperatures at which 5% and 10% weight losses occur ($T_{5\%}$ and $T_{10\%}$, respectively) are found to increase significantly upon succinylation irrespective of the SAn/SLF ratio (see Table 3),

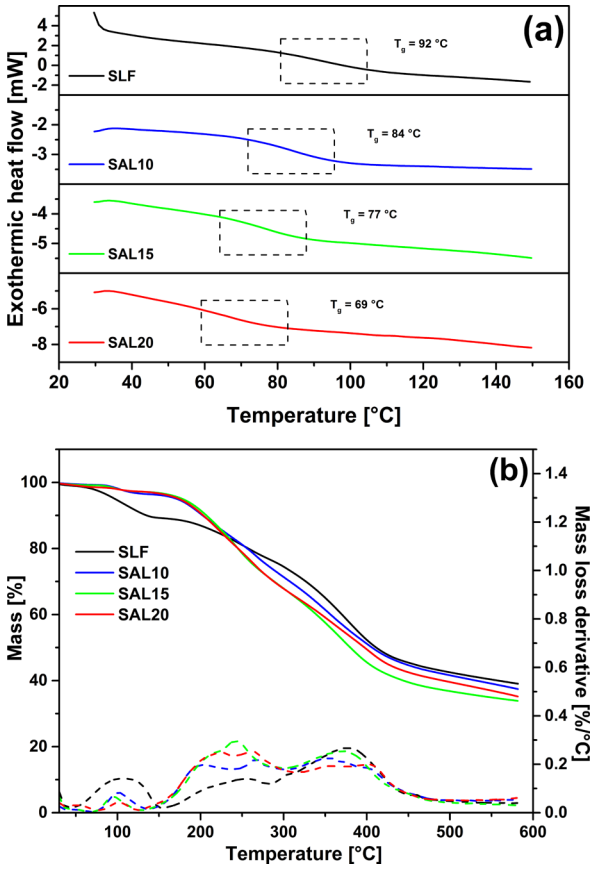

Figure 2. (a) DSC and (b) TGA/dTGA scans of THF-soluble lignin fraction (SLF) and of SAn-based adducts (SAL10, SAL15, SAL20) performed under nitrogen flux.

Table 3. Thermal Degradation Temperatures at 5% ($T_{5\%}$), 10% ($T_{10\%}$), Second Mass Loss Event Onset (T_{ON}), and 50% ($T_{50\%}$) Mass Loss, Final Char Residue at 570 °C (R_{570}), and Maximum Mass Loss Derivative Temperature (T_{DTGmax}) for SAn-Based Lignin Adducts[a]

	$T_{5\%}$ [°C]	$T_{10\%}$ [°C]	T_{ON} [°C]	$T_{50\%}$ [°C]	R_{570} [%]	T_{DTGmax} [°C]
SLF	97	135	154	411	39.6	376
SAL10	171	202	137	406	38.1	357
SAL15	178	207	130	380	34.2	243
SAL20	174	203	125	397	35.8	264

[a]As measured by TGA under N_2 stream. For comparison, data for the unmodified material (SLF) are also presented.

although a slightly lower thermal degradation onset temperature (T_{ON}) is observed on SAL adducts compared with SLF in the temperature range covering the second mass loss event (150−300 °C). This behavior may be correlated with the increased molecular weight of these systems resulting from the addition of the ester moieties to the lignin macromolecule (Table 1), which also appears to reduce moisture uptake in the functionalized materials (a lower mass loss derivative in the 25−150 °C temperature range is observed on SAL systems as opposed to SLF). On the other hand, in the higher temperature range (>250−300 °C), complex mass loss events are observed for all SAL systems, ultimately leading to a thermal degradation response which is found to be comparable to that observed on untreated SLF. In this respect, similar values of $T_{50\%}$ (thermal degradation temperature at 50% mass loss) and R_{570} (final char residue at 570 °C) are obtained for SAn-based lignin adducts and unmodified lignin. The thermo-oxidative behavior of lignin fractions was examined by means of TGA under air flux (Supporting Information). A lower thermal stability of SLF in air was observed compared to all SAn-based adducts for temperatures lower than 250 °C, likely ascribable to significant loss of adsorbed moisture in the pristine material. By further increasing the temperature (T > 250 °C), all SAn-based adducts exhibited similar thermo-oxidative profiles, leading to a R_{570} value of around 1−2%, as a result of the complete disruption of the macromolecular chains due to high-temperature thermal oxidation.

FTIR on lignin-based PE coatings. Based on the trends observed on succinylated systems as discussed above, SAL20 was selected as starting building block for the formation of lignin-based thermosetting PE coatings. To this end, two different cross-linking strategies were explored: in the first approach, SAL20 was cross-linked with small amounts of a melamine-based curing agent (HMMM) at increasing SAL/HMMM ratios, namely 93/7 (SAL-H7), 95/5 (SAL-H5), and 97/3 (SAL-H3); in the second approach, a self-polyesterification reaction was conducted in which the carboxyl groups in SAL20 were allowed to react with the residual hydroxyl groups still present in the lignin-based adduct as a result of the incomplete conversion of the mild reaction with SAn (see Figure 1 and discussion thereof). Cross-linking was performed at 200 °C for 30 min. In the latter case, a potentially 100%-renewable-carbon-based polymer coating could be produced, in addition to avoiding the use of derivatives of substances of very high concern (such as formaldehyde, in the case of HMMM) and preventing the emission of volatile organic substances in the atmosphere (the byproduct of the curing polyesterification reaction of the SAn-based adduct is water).

FTIR spectroscopy was used to monitor the reaction between SAL20 and HMMM as well as the self-polyesterification process and to investigate the chemical structure of the resulting lignin-based PE films. As observed in Figure 3a, where the FTIR spectra of all lignin-based cross-linked systems are presented, all materials exhibit a decrease of signal intensity in the 3400−3000 cm^{-1} spectral region compared to the pristine SAn-based lignin adduct SAL20. This modification, observed on both SAL-S and all SAL-Hx systems, may be correlated with a decrease of the O−H stretching vibrations in these materials as a result of the occurring cross-linking reaction. On the other hand, the characteristic signals of HMMM can be observed in the FTIR spectra of all SAL-Hx systems,[50] suggesting successful incorporation of the co-curing agent in the final cross-linked materials (Figure 3b). In particular, a peak at the 3412 cm^{-1} is found to appear upon reaction between SAL20 and HMMM (with increasing intensity for higher HMMM contents), attributable to stretching vibrations of free secondary amines and imines. In addition, two bands at 1545 and 1484 cm^{-1} (typically associated with the in plane deformations of C═N in the 1,3,5-triazine ring) are observed on the co-cured materials, whose intensity is found to decrease by increasing the SAL/HMMM ratio (i.e., by decreasing the amount of HMMM in the polymer). Similarly, a progressive broadening of the signal in the 1350−1300 cm^{-1} range is also observed by increasing HMMM content, likely resulting from the signals associated with C−N stretching vibrations observable in the same spectral region in pure HMMM. Finally, the signal characteristic of O−CH_3 stretching vibrations in HMMM and peaked at 2818 cm^{-1}

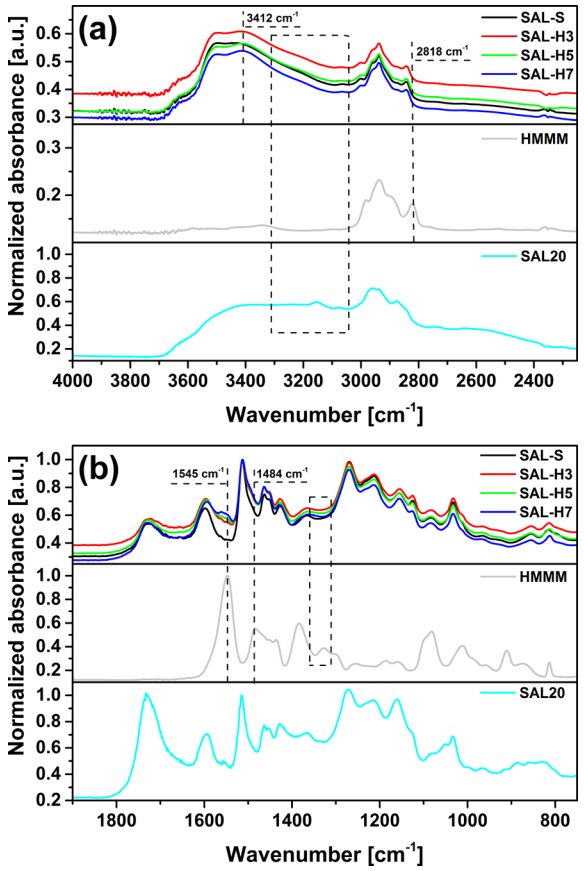

Figure 3. FTIR spectra of lignin-based cross-linked polyester systems (SAL-S, SAL-H3, SAL-H5, SAL-H7) between (a) 4000−2250 cm^{-1} (dashed area highlights the 3400−3100 cm^{-1} spectral region) and (b) 1900−750 cm^{-1} (dashed area highlights the 1350−1300 cm^{-1} spectral region). The FTIR spectra of HMMM and SAL20 are also reported for easy reference.

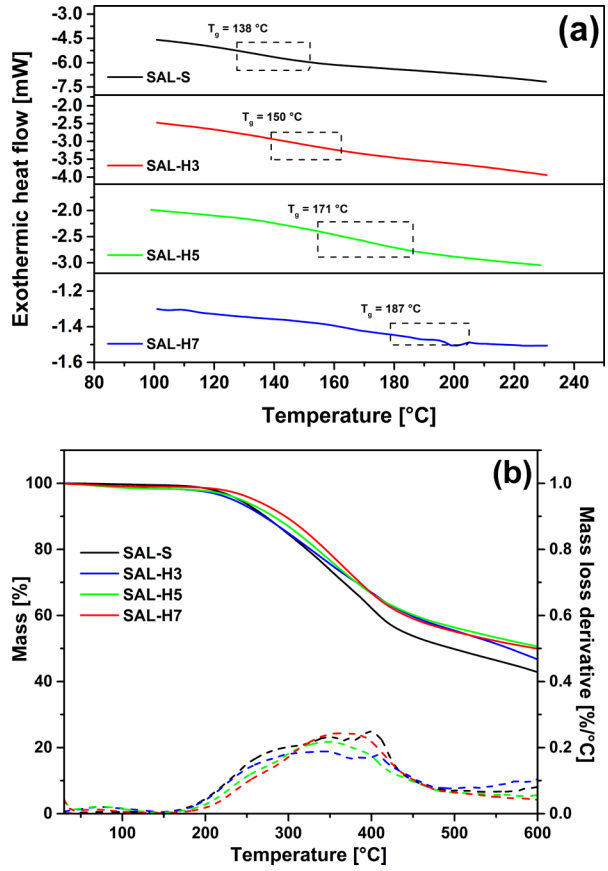

Figure 4. (a) DSC traces and (b) TGA profiles under nitrogen flux of lignin-based cross-linked polyester systems SAL-S, SAL-H3, SAL-H5, and SAL-H7 (the enthalpic step at T_g was found to be 0.14 W/g, 0.11 W/g, 0.07 W/g, and 0.02 W/g for SAL-S, SAL-H3, SAL-H5, and SAL-H7, respectively).

is found to disappear in all SAL-Hx systems (irrespective of the SAL/HMMM ratio). This evidence clearly indicates successful polyetherification condensation reaction between methoxy groups in HMMM and hydroxyl groups in SAL20, ultimately leading to the covalent incorporation of the curing agent in the final cross-linked materials.

Experimental evidence of the successful progress of the cross-linking reaction was also obtained by testing the solvent resistance of all polyester coatings (SAL-S and all SAL-Hx systems) via the MEK double rub test.[51] All materials were found to withstand more than 100 MEK double rubs, suggesting the presence of a fully chemically cross-linked structure irrespective of the chemistry of the cross-linking process. In addition, supplementary tests were carried out to evaluate further the extent of cross-linking, by immersing the PE films in MEK and in THF for 24 h and by gravimetrically assessing the extracted soluble fraction. In all cases, more than 99% of insoluble material was found after immersion, clearly indicating excellent solvent resistance of all systems.

Thermal characterization of lignin-based PE coatings. To investigate the thermal transitions in the lignin-based cross-linked polyester materials, DSC analysis was performed on SAL-S and all SAL-Hx systems. As shown in Figure 4a, upon cross-linking, an increase of T_g is found in all materials compared with the unreacted SAL20 adduct. In particular, a T_g of 138 °C is observed on the self-cross-linked material (SAL-S). Similarly, the melamine-based cross-linked systems exhibit T_g values of 150 °C, 171 °C, and 187 °C for SAL-H3, SAL-H5, and SAL-H7, respectively, with no evidence of phase segregation (only one T_g is observed). Such a sharp increase in T_g, which is found to scale with the amount of HMMM in the PE material, can be rationalized on the basis of the increasing density of cross-linking at increasing HMMM content. To gain further insights in the relation between the chemical composition of the SAL-Hx systems and their calorimetric response, the T_g values obtained via DSC measurements were compared with those predicted by the simplified Couchman−Karasz equation (Supporting Information).[52] As recently observed on analogous lignin-based polymeric systems,[13] strong positive deviations from the theoretical behavior were observed that may be correlated with changes in the enthalpy and excess entropy of mixing in the system at the glass-to-liquid transition,[53−55] likely resulting from the increased influence of intermolecular hydrogen bonding interactions within the co-cross-linked systems.

The thermal stability of the PE materials was investigated by means of TGA measurements. As presented in Figure 4b, all cross-linked systems exhibit a thermolytic degradation profile characterized by the presence of a major mass loss event occurring in the 200−500 °C temperature range, while excellent stability is observed below 200 °C. Indeed, $T_{5\%}$ values of 241 °C, 233 °C, 243 °C, and 259 °C are obtained on SAL-S, SAL-H3, SAL-H5, and SAL-H7, respectively. A

Table 4. Static Contact Angles (θ_{H2O}, θ_{CH2I2}), Total Surface Tension (γ), and Corresponding Dispersive (γ^d) and Polar (γ^p) Components of Cross-linked PE Systems[a]

	θ_{H2O} [deg]	θ_{CH2I2} [deg]	γ [mN/m]	γ^d [mN/m]	γ^p [mN/m]
SAL-S	89.9 ± 2.7	47.7 ± 2.3	35.9 ± 0.2	2.3 ± 0.4	33.6 ± 0.3
SAL-H3	94.3 ± 1.9	50.1 ± 3.5	34.3 ± 0.3	1.4 ± 0.1	32.9 ± 0.2
SAL-H5	100.3 ± 0.9	56.6 ± 3.0	30.5 ± 0.1	0.7 ± 0.2	29.8 ± 0.4
SAL-H7	98.8 ± 1.1	53.0 ± 5.3	32.6 ± 0.4	0.7 ± 0.2	31.8 ± 0.3

[a]Average values ± standard deviation out of at least 20 measurements.

slightly higher thermal stability is observed at 600 °C in co-cured systems with respect to SAL-S, as evidenced by the higher char residue recovered at 600 °C (see Supporting Information for numerical values of characteristic thermal degradation temperatures). It is interesting to note that, compared with the pristine succinylated material (SAL20, Figure 2b and Table 3), all cured systems are characterized by significantly improved thermal stability in the low-temperature range (<200 °C) as a result of the presence of the three-dimensional cross-linked structure that allows notable extension of the applicability of these materials to a broader temperature range, in line with the typical thermal stability of conventional fossil-based systems[56] (analogous trends are also found in TGA measurements performed in air, as detailed in the Supporting Information).

Surface and mechanical characterization of lignin-based PE coatings. The surface wettability properties of the cross-linked lignin-based polyester materials were investigated by means of contact angle measurements using water and diiodomethane as probe liquids. The results are listed in Table 4, where the resulting values of surface tension γ of each system together with their corresponding dispersive (γ^d) and polar (γ^p) components are also presented, as calculated with the Owens, Wendt, Rabel, and Kaelble (OWRK) method.[57] All samples are found to be of hydrophobic nature, with water contact angles (θ_{H2O}) in the 90−100° range. In particular, slightly higher θ_{H2O} values are found on SAL/HMMM co-cured systems, where an increasing amount of lignin leads to lower water repellence (θ_{H2O} = 94.3°, 100.3°, and 98.8° for SAL-H3, SAL-H5, and SAL-H7, respectively), although no clear trends can be observed. This behavior may be correlated with the higher polarity of lignin compared with HMMM as a result of the presence of (unreacted) hydroxyl groups in its structure which increase in number for increasing SAL/HMMM ratios (as confirmed also by FTIR analysis, see Figure 3). As a result, stronger surface interactions with water can be established that lead to lower θ_{H2O} in these systems. Indeed, among the co-cured systems, both γ and γ^p are found to be maximum in SAL-H3 (γ = 34.3 mN/m and γ^p = 32.9 mN/m). Accordingly, a further increase in γ and γ^p is observed in SAL-S (γ = 35.9 mN/m and γ^p = 33.6 mN/m), as expected.

In order to assess the suitability of the lignin-based PE systems for application as bioderived coating materials in the manufacturing field, a further investigation was conducted on their viscoelastic response and surface mechanical properties at the nanoscale. To this end, dynamic hardness measurements were obtained through nanoscratch resistance tests performed by means of an atomic force microscopy (AFM) system, equipped with a lithographic module. In line with the objective of obtaining biobased coating materials with high lignin content, these measurements were performed only on SAL-S and SAL-H3 systems, which are characterized by the highest amount of renewable carbon. Figure 5 shows some examples of

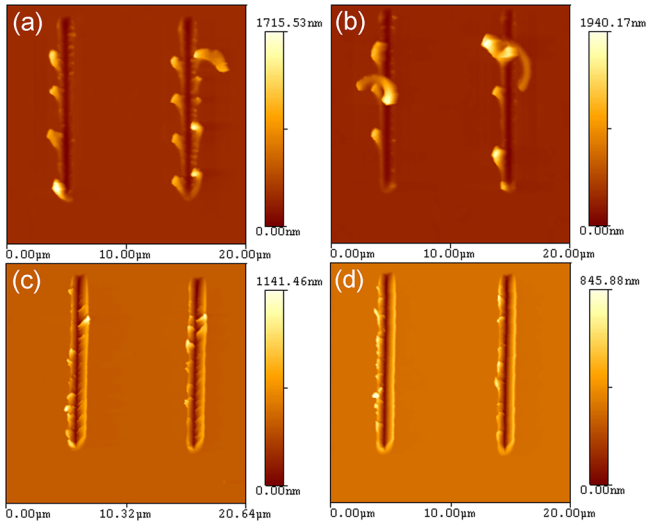

Figure 5. AFM height images (20 μm × 20 μm) of scratches performed on self-cross-linked PE coatings (SAL-S, (a) and (b)) and on high-lignin-content PE coatings cross-linked with a HMMM (SAL-H3, (c) and (d)), recorded at two different nanoscratch rates: (a) and (c) at 0.1 μm/s; (b) and (d) at 10 μm/s.

scratches obtained on SAL-S and SAL-H3 coatings and performed at two different scratch rates (0.1 μm/s and 10 μm/s) by means of an AFM nanoindentation probe. A large amount of debris was visible on SAL-S samples at the bottom of the scratches as well as along the grooves (Figure 5a and b). In this case, the scratch deformation mechanism appeared to be completely brittle with the formation of chips detached and pushed either to the end or to the sides of the grooves. A brittle scratch deformation was also observed for SAL-H3; however, it was characterized by a lower amount of debris and regular cracks (Figure 5c and d). To evaluate the effect of the succinylation strategy on the resulting mechanical properties of the lignin-based PE coatings, nanoscratch tests were performed also on coatings obtained by using unmodified pristine SLF (no functionalization with SAn performed) and HMMM with a SLF/HMMM ratio of 97/3 (SLF-H3). In this case, a very brittle behavior associated with a large amount of chips was evidenced, clearly highlighting the importance of the SAn-based functionalization step to achieve materials of improved toughness (see Supporting Information). As for SAL-H3, the material flowed around the nanoindenter, forming more uniform grooves with ridges more homogeneously distributed along the sides of the scratches, when compared with SAL-S coatings. This suggests that SAL-H3 coatings exhibit some plastic deformation mechanism, being similar to that of a plowed material.

The calculation of the dynamic hardness values of the analyzed coatings (Table 5) revealed that SAL-S and SAL-H3 have similar values of dynamic hardness measured at a

Table 5. Dynamic Hardness (H_d) and Average Penetration Depth (D_p) Measured through AFM-Based Nanoscratch Tests at Different Nanoscratch Rates (0.1 μm/s and 10 μm/s) and Adhesive Strength Obtained by Pull-off Test on High-Lignin-Content PE Coatings SAL-S and SAL-H3 (average values ± standard deviation out of 4 measurements)

	nanoscratch rate 0.1 μm/s		nanoscratch rate 10 μm/s		pull-off adhesive strength		
	H_d [GPa]	D_p [nm]	H_d [GPa]	D_p [nm]	wood [MPa]	glass [MPa]	aluminum [MPa]
SAL-S	0.52 ± 0.16	210 ± 49	0.53 ± 0.09	182 ± 18	>9[a]	6.5 ± 0.4	1.0 ± 0.1
SAL-H3	0.63 ± 0.06	275 ± 30	0.64 ± 0.04	266 ± 11	>9[a]	5.7 ± 0.1	1.4 ± 0.1

[a]Cohesive detachment of the substrate (9 MPa represents the maximum allowable instrumental reading).

scratching rate of 0.1 μm/s. This highlights the possibility to obtain 100% biobased coatings with a good level of hardness, comparable with those cross-linked with curing agents from synthetic sources. Dynamic hardness was also measured on SLF-H3 coatings (containing unfunctionalized lignin), and a lower value of hardness (0.42 ± 0.07 GPa) was observed in comparison with SAL-S and SAL-H3. These results indicate that the functionalization of lignin with SAn enables an enhancement of coating hardness, with values in line with analogous fossil-based PE coating systems.[58] Time-dependent effects on hardness values were investigated by performing the scratch tests with two different indenter rates. As shown in Table 5, the nanoscratch hardness of SAL-H3 and SAL-S systems did not appear to be affected by the nanoindenter rate. Unlike SAL systems, SLF-H3 coatings exhibited a higher value of hardness by increasing the probe rate (0.51 ± 0.01 GPa). The dependence of scratch hardness upon the nanoscratch rate suggests the viscoelastic-plastic nature of SLF-H3 coatings. Conversely, the mechanical behavior appears to be scarcely viscoelastic for SAL-based systems. This is likely due to the functional succinylated lignin adducts, which make reactive sites more accessible during cross-linking, reducing steric hindrance and thus increasing the degree of cross-linking in the biobased PE coatings.

Following the assessment of the surface viscoelastic properties of the high-lignin-content PE systems by means of dynamic hardness measurements, their adhesive strength was evaluated by performing pull-off tests[45] on coatings deposited on different substrates, namely wood, glass, and aluminum. As reported in Table 5, maximum adhesion was observed on wood, where cohesive detachment of the substrate occurred during the test as a result of the intimate coating/substrate interactions arising from the lignocellulosic nature of these PE materials.[59] On glass, values of adhesive strength of 6.5 and 5.7 MPa were reported for SAL-S and SAL-H3, respectively. This positive behavior may be correlated with the presence of noncovalent interactions (viz., hydrogen bonds) establishing between polar groups in the lignin-based cross-linked formulations and the available oxygen groups present on the glass surface. On the contrary, slightly lower adhesion strengths were obtained on aluminum (1.0 and 1.4 MPa for SAL-S and SAL-H3, respectively), which are however in line with typical values obtained with conventional fossil-based PE coatings on untreated metal coils.[60]

CONCLUSIONS

New high-lignin-content thermosetting PE coating materials were developed and presented in this study. These new systems were based on the preliminary functionalization of a THF-soluble fraction of softwood kraft lignin with increasing amounts of SAn to obtain lignin/SAn adducts (SAL) via the formation of ester bonds on the hydroxyl groups in lignin. Upon succinylation, an increase in molecular weight was consistently observed, as a result of the incorporation of lateral chains (from SAn) to the main lignin macromolecular backbone. FTIR spectroscopy showed that the esterification reaction resulted in a decrease of the OH-group signal intensity in lignin (3400 cm^{-1}), along with the appearance of a major absorption band at 1700 cm^{-1} (C═O stretching in ester groups). In addition, a maximum SAn/lignin feed ratio could be identified that allowed exclusion of any presence of unreacted anhydride in the reaction product. Thermogravimetric and calorimetric analyses evidenced an improved thermal stability in the functionalized SAL systems compared with the pristine material, in addition to a progressive decrease in T_g by increasing the SAn/lignin ratio resulting from the plasticization effect of SAn on lignin. The succinylated adducts were subsequently employed as building blocks to obtain fully cross-linked lignin-based PE coatings by resorting to two different cross-linking strategies, namely (1) reaction in the presence of small amounts of a HMMM-based curing agent and (2) self-polyesterification. Calorimetric analysis suggested that the cross-linking reaction successfully occurred for both approaches, as evidenced by the significant increase in T_g for the reacted materials as compared with the parent system. Similarly, the thermal stability of the coatings was found to improve significantly upon cross-linking. The surface wettability of the polyester systems was investigated by means of contact angle measurements, and improved hydrophobicity was found on all coatings, with higher water repellence observed on SAL/HMMM co-cured systems. To assess the suitability of such materials as highly performing bioderived coatings in the manufacturing field, a further investigation was conducted on their viscoelastic response and surface mechanical properties at the nanoscale. To this end, dynamic hardness measurements obtained by means of nanoscratch resistance tests on high-lignin-content systems revealed a high level of hardness (around 0.6 GPa), likely due to a good degree of cross-linking. Finally, these systems were found to exhibit high adhesion strength on different substrates.

The results of this study provide a clear demonstration of an easily accessible and widely applicable strategy to develop high-lignin-content thermosetting PE systems and highlight the potential of lignin-based PE thermosets as bioderived coatings and adhesives.

The Supporting Information is available free of charge on the ACS Publications website at DOI: 10.1021/acssuschemeng.7b03583.

GPC chromatograms of SAn-based lignin adducts; FTIR spectra of SLF-, SAn-, and SAn-based adducts SAL20 and SAL25; ^{31}P NMR spectra of pristine softwood kraft

lignin (KL), THF-soluble lignin fraction (SLF), and SAL20 adduct (SAL20); TGA and dTGA scans of SLF and of SAn-based adducts (SAL10, SAL15, SAL20) performed in air; DSC scan of HMMM after thermal treatment; dependence of T_g on lignin mass fraction as obtained from the Couchman−Karasz equation and from experimental DSC measurements; thermal degradation temperatures for cross-linked polyester systems under N_2 and air stream; TGA/dTGA scans of lignin-based cross-linked polyester systems (SAL-S, SAL-H3, SAL-H5, SAL-H7) performed under air flux; TGA/dTGA scans of HMMM in air and N_2; experimental procedure for measuring the dynamic hardness of the coatings; AFM height images of scratches performed on biobased PE coatings obtained using SLF and a SLF/HMMM ratio of 97/3 (SLF-H3) (PDF)

ACKNOWLEDGMENTS

This project was funded by the European Commission's Seventh Framework Programme for research, technological development and demonstration under grant agreement no FP7-KBBE-2013-7-613802 ("*ValorPlus - Valorisation of bio-refinery by-products leading to closed loop systems with improved economic and environmental performance*"). The authors gratefully acknowledge Gigliola Clerici for support with GPC and thermal analysis, and Juan Carlos de Haro Sanchez for support with ^{31}P NMR analysis.

REFERENCES

(1) Isikgor, F. H.; Becer, C. R. Lignocellulosic biomass: a sustainable platform for the production of bio-based chemicals and polymers. *Polym. Chem.* **2015**, *6* (25), 4497−4559.

(2) Ragauskas, A. J.; Beckham, G. T.; Biddy, M. J.; Chandra, R.; Chen, F.; Davis, M. F.; Davison, B. H.; Dixon, R. A.; Gilna, P.; Keller, M.; Langan, P.; Naskar, A. K.; Saddler, J. N.; Tschaplinski, T. J.; Tuskan, G. A.; Wyman, C. E. Lignin Valorization: Improving Lignin Processing in the Biorefinery. *Science* **2014**, *344* (6185), 1246843.

(3) Tuck, C. O.; Pérez, E.; Horváth, I. í. T.; Sheldon, R. A.; Poliakoff, M. Valorization of Biomass: Deriving More Value from Waste. *Science* **2012**, *337* (6095), 695−699.

(4) Lora, J.; Glasser, W. Recent Industrial Applications of Lignin: A Sustainable Alternative to Nonrenewable Materials. *J. Polym. Environ.* **2002**, *10* (1−2), 39−48.

(5) Belgacem, M. N.; Blayo, A.; Gandini, A. Organosolv lignin as a filler in inks, varnishes and paints. *Ind. Crops Prod.* **2003**, *18* (2), 145−153.

(6) Lora, J. Industrial Commercial Lignins: Sources, Properties and Applications. In *Monomers, Polymers and Composites from Renewable Resources*; Belgacem, M. N., Gandini, A., Eds.; Elsevier: Amsterdam, The Netherlands, 2008; Chapter 10, pp 225−241.

(7) Cateto, C. A.; Barreiro, M. F.; Rodrigues, A. E.; Brochier-Solan, M. C.; Thielemans, W.; Belgacem, M. N. Lignins as macromonomers for polyurethane synthesis: A comparative study on hydroxyl group determination. *J. Appl. Polym. Sci.* **2008**, *109* (5), 3008−3017.

(8) Doherty, W. O. S.; Mousavioun, P.; Fellows, C. M. Value-adding to cellulosic ethanol: Lignin polymers. *Ind. Crops Prod.* **2011**, *33* (2), 259−276.

(9) Duval, A.; Lawoko, M. A review on lignin-based polymeric, micro- and nano-structured materials. *React. Funct. Polym.* **2014**, *85* (0), 78−96.

(10) Gandini, A.; Belgacem, M. N. Lignins as Components of Macromolecular Materials. In *Monomers, Polymers and Composites from Renewable Resources*; Belgacem, M. N., Gandini, A., Eds.; Elsevier: Amsterdam, The Netherlands, 2008; Chapter 11, pp 243−271.

(11) Laurichesse, S.; Avérous, L. Chemical modification of lignins: Towards biobased polymers. *Prog. Polym. Sci.* **2014**, *39* (7), 1266−1290.

(12) Thakur, V. K.; Thakur, M. K.; Raghavan, P.; Kessler, M. R. Progress in Green Polymer Composites from Lignin for Multifunctional Applications: A Review. *ACS Sustainable Chem. Eng.* **2014**, *2* (5), 1072−1092.

(13) Griffini, G.; Passoni, V.; Suriano, R.; Levi, M.; Turri, S. Polyurethane Coatings Based on Chemically Unmodified Fractionated Lignin. *ACS Sustainable Chem. Eng.* **2015**, *3* (6), 1145−1154.

(14) Upton, B. M.; Kasko, A. M. Strategies for the Conversion of Lignin to High-Value Polymeric Materials: Review and Perspective. *Chem. Rev.* **2016**, *116* (4), 2275−2306.

(15) Kai, D.; Tan, M. J.; Chee, P. L.; Chua, Y. K.; Yap, Y. L.; Loh, X. J. Towards lignin-based functional materials in a sustainable world. *Green Chem.* **2016**, *18* (5), 1175−1200.

(16) Vilela, C.; Sousa, A. F.; Fonseca, A. C.; Serra, A. C.; Coelho, J. F. J.; Freire, C. S. R.; Silvestre, A. J. D. The quest for sustainable polyesters - insights into the future. *Polym. Chem.* **2014**, *5* (9), 3119−3141.

(17) Evtugin, D. V.; Gandini, A. Polyesters based on oxygen-organosolv lignin. *Acta Polym.* **1996**, *47* (8), 344−350.

(18) Guo, Z.-X.; Gandini, A. Polyesters from lignin—2. The copolyesterification of kraft lignin and polyethylene glycols with dicarboxylic acid chlorides. *Eur. Polym. J.* **1991**, *27* (11), 1177−1180.

(19) Guo, Z.-X.; Gandini, A.; Pla, F. Polyesters from lignin. 1. The reaction of kraft lignin with dicarboxylic acid chlorides. *Polym. Int.* **1992**, *27* (1), 17−22.

(20) Luong, N.; Binh, N.; Duong, L.; Kim, D.; Kim, D. S.; Lee, S.; Kim, B.; Lee, Y.; Nam, J. D. An eco-friendly and efficient route of lignin extraction from black liquor and a lignin-based copolyester synthesis. *Polym. Bull.* **2012**, *68* (3), 879−890.

(21) Thanh Binh, N. T.; Luong, N. D.; Kim, D. O.; Lee, S. H.; Kim, B. J.; Lee, Y. S.; Nam, J. D. Synthesis of Lignin-Based Thermoplastic Copolyester Using Kraft Lignin as a Macromonomer. *Compos. Interfaces* **2009**, *16* (7−9), 923−935.

(22) Bonini, C.; D'Auria, M.; Emanuele, L.; Ferri, R.; Pucciariello, R.; Sabia, A. R. Polyurethanes and polyesters from lignin. *J. Appl. Polym. Sci.* **2005**, *98* (3), 1451−1456.

(23) Kang, Y.; Chen, Z.; Wang, B.; Yang, Y. Synthesis and mechanical properties of thermoplastic films from lignin, sebacic acid and poly(ethylene glycol). *Ind. Crops Prod.* **2014**, *56* (0), 105−112.

(24) Thielemans, W.; Wool, R. P. Lignin Esters for Use in Unsaturated Thermosets: Lignin Modification and Solubility Modeling. *Biomacromolecules* **2005**, *6* (4), 1895−1905.

(25) Maldhure, A. V.; Chaudhari, A. R.; Ekhe, J. D. Thermal and structural studies of polypropylene blended with esterified industrial waste lignin. *J. Therm. Anal. Calorim.* **2011**, *103* (2), 625−632.

(26) Monteil-Rivera, F.; Paquet, L. Solvent-free catalyst-free microwave-assisted acylation of lignin. *Ind. Crops Prod.* **2015**, *65*, 446−453.

(27) Kaewtatip, K.; Thongmee, J. Effect of kraft lignin and esterified lignin on the properties of thermoplastic starch. *Mater. Eng.* **2013**, *49*, 701−704.

(28) Sailaja, R. R. N.; Deepthi, M. V. Mechanical and thermal properties of compatibilized composites of polyethylene and esterified lignin. *Mater. Eng.* **2010**, *31* (9), 4369−4379.

(29) Fox, S. C.; McDonald, A. G. Chemical and thermal characterization of three industrial lignins and their corresponding lignin esters. *BioResources* **2010**, *5* (2), 990−1009.
(30) Chen, Q.; Ni, Y.; He, Z. Using cationic polymers to improve alkenyl succinic anhydride (asa) sizing efficiency in high-yield pulp containing furnish. *BioResources* **2012**, *7* (3), 3948−3959.
(31) Lindfors, J.; Salmi, J.; Laine, J.; Stenius, P. AKD and ASA model surfaces: preparation and characterization. *BioResources* **2007**, *2* (4), 652−670.
(32) Bechthold, I.; Bretz, K.; Kabasci, S.; Kopitzky, R.; Springer, A. Succinic Acid: A New Platform Chemical for Biobased Polymers from Renewable Resources. *Chem. Eng. Technol.* **2008**, *31* (5), 647−654.
(33) Delhomme, C.; Weuster-Botz, D.; Kuhn, F. E. Succinic acid from renewable resources as a C4 building-block chemical-a review of the catalytic possibilities in aqueous media. *Green Chem.* **2009**, *11* (1), 13−26.
(34) Bridson, J. H.; van de Pas, D. J.; Fernyhough, A. Succinylation of three different lignins by reactive extrusion. *J. Appl. Polym. Sci.* **2013**, *128* (6), 4355−4360.
(35) Xiao, B.; Sun, X. F.; Sun, R. The chemical modification of lignins with succinic anhydride in aqueous systems. *Polym. Degrad. Stab.* **2001**, *71* (2), 223−231.
(36) Hirose, S.; Hatakeyama, T.; Hatakeyama, H. Synthesis and thermal properties of epoxy resins from ester-carboxylic acid derivative of alcoholysis lignin. *Macromol. Symp.* **2003**, *197* (1), 157−170.
(37) Hirose, S.; Hatakeyama, T.; Hatakeyama, H. Curing and Glass Transition of Epoxy Resins from Ester-Carboxylic Acid Derivatives of Mono- and Disaccharides, and Alcoholysis Lignin. *Macromol. Symp.* **2005**, *224* (1), 343−354.
(38) Ismail, T. N. M. T.; Hassan, H. A.; Hirose, S.; Taguchi, Y.; Hatakeyama, T.; Hatakeyama, H. Synthesis and thermal properties of ester-type crosslinked epoxy resins derived from lignosulfonate and glycerol. *Polym. Int.* **2010**, *59* (2), 181−186.
(39) Qin, J.; Woloctt, M.; Zhang, J. Use of Polycarboxylic Acid Derived from Partially Depolymerized Lignin As a Curing Agent for Epoxy Application. *ACS Sustainable Chem. Eng.* **2014**, *2* (2), 188−193.
(40) Passoni, V.; Scarica, C.; Levi, M.; Turri, S.; Griffini, G. Fractionation of Industrial Softwood Kraft Lignin: Solvent Selection as a Tool for Tailored Material Properties. *ACS Sustainable Chem. Eng.* **2016**, *4* (4), 2232−2242.
(41) Balakshin, M.; Capanema, E. On the quantification of lignin hydroxyl groups with ^{31}P and ^{13}C NMR spectroscopy. *J. Wood Chem. Technol.* **2015**, *35* (3), 220−237.
(42) Suriano, R.; Oldani, V.; Bianchi, C. L.; Turri, S. AFM nanomechanical properties and durability of new hybrid fluorinated sol-gel coatings. *Surf. Coat. Technol.* **2015**, *264*, 87−96.
(43) Williams, J. A. Analytical models of scratch hardness. *Tribol. Int.* **1996**, *29* (8), 675−694.
(44) Graça, S.; Colaço, R.; Vilar, R. Micro-to-Nano Indentation and Scratch Hardness in the Ni−Co System: Depth Dependence and Implications for Tribological Behavior. *Tribol. Lett.* **2008**, *31* (3), 177.
(45) Standard Test Method for Pull-Off Strength of Coatings Using Portable Adhesion Testers. ASTM D4541-09, 2009.
(46) Faix, O. Fourier Transform Infrared Spectroscopy. In *Methods in Lignin Chemistry*; Lin, S. Y., Dence, C. W., Eds.; Springer-Verlag: Heidelberg, Germany, 1992; pp 233−241.
(47) Koivu, K. A. Y.; Sadeghifar, H.; Nousiainen, P. A.; Argyropoulos, D. S.; Sipilä, J. Effect of Fatty Acid Esterification on the Thermal Properties of Softwood Kraft Lignin. *ACS Sustainable Chem. Eng.* **2016**, *4* (10), 5238−5247.
(48) Ciobanu, C.; Ungureanu, M.; Ignat, L.; Ungureanu, D.; Popa, V. I. Properties of lignin-polyurethane films prepared by casting method. *Ind. Crops Prod.* **2004**, *20* (2), 231−241.
(49) Domínguez, J. C.; Oliet, M.; Alonso, M. V.; Gilarranz, M. A.; Rodríguez, F. Thermal stability and pyrolysis kinetics of organosolv lignins obtained from Eucalyptus globulus. *Ind. Crops Prod.* **2008**, *27* (2), 150−156.
(50) Larkin, P. J.; Makowski, M. P.; Colthup, N. B.; Flood, L. A. Vibrational analysis of some important group frequencies of melamine derivatives containing methoxymethyl, and carbamate substituents: mechanical coupling of substituent vibrations with triazine ring modes. *Vib. Spectrosc.* **1998**, *17* (1), 53−72.
(51) Standard Practice for Assessing the Solvent Resistance of Organic Coatings Using Solvent Rubs. ASTM D5402-93, 1999.
(52) Couchman, P. R.; Karasz, F. E. A Classical Thermodynamic Discussion of the Effect of Composition on Glass-Transition Temperatures. *Macromolecules* **1978**, *11* (1), 117−119.
(53) Painter, P. C.; Graf, J. F.; Coleman, M. M. Effect of hydrogen bonding on the enthalpy of mixing and the composition dependence of the glass transition temperature in polymer blends. *Macromolecules* **1991**, *24* (20), 5630−5638.
(54) Pinal, R. Entropy of Mixing and the Glass Transition of Amorphous Mixtures. *Entropy* **2008**, *10* (3), 207.
(55) Lienhard, D. M.; Zobrist, B.; Zuend, A.; Krieger, U. K.; Peter, T. Experimental evidence for excess entropy discontinuities in glass-forming solutions. *J. Chem. Phys.* **2012**, *136* (7), 074515.
(56) Narayan, R.; Chattopadhyay, D. K.; Sreedhar, K.; Raju, V. S. N.; Mallikarjuna, N. N.; Aminabhavi, T. M. Degradation Profiles of Polyester-Urethane (HP-MDI) and Polyester-Melamine (HP-HMMM) Coatings: A Thermal Study. *J. Appl. Polym. Sci.* **2005**, *97* (2), 518−526.
(57) Chan, C.-M. *Polymer surface modification and characterization*; Hanser Gardner Publications: Munich, 1993.
(58) Frings, S.; van Nostrum, C. F.; van der Linde, R.; Meinema, H. A.; Rentrop, C. H. A. Morphology of hybrid coatings based on polyester, melamine resin, and silica and the relation with hardness and scratch resistance. *J. Coat. Technol.* **2000**, *72* (901), 83−89.
(59) Köhler, R.; Sauerbier, P.; Militz, H.; Viöl, W. Atmospheric Pressure Plasma Coating of Wood and MDF with Polyester Powder. *Coatings* **2017**, *7* (10), 171.
(60) Bajat, J. B.; Popić, J. P.; Mišković-Stanković, V. B. The influence of aluminium surface pretreatment on the corrosion stability and adhesion of powder polyester coating. *Prog. Org. Coat.* **2010**, *69* (4), 316−321.